Analyst

ROYAL SOCIETY OF CHEMISTRY

PAPER

View Article Online
View Journal | View Issue

Cite this: *Analyst*, 2025, **150**, 1571

CRISPR/Cas12a-powered nanoconfined biosensing platform with hybrid chain reaction cascading guanine nanowire amplification for ultrasensitive dual-mode detection of lipopolysaccharide†

Yanlei Li,[a] Xiang Ren,[a] Dan Wu,[a] Hongmin Ma,[a] Qin Wei,[a,b] Huangxian Ju[a,c] and Zhongfeng Gao *[a]

Traditional endotoxin detection methods face challenges in sensitivity, interference resistance, and reliability. This study develops a CRISPR/Cas12a-powered nanoconfined biosensing system that integrates mesoporous nanoengineering with a hybrid chain reaction (HCR) cascading guanine nanowire (G-wire) dual amplification strategy for ultrasensitive dual-mode detection of lipopolysaccharide (LPS). By leveraging a vertically ordered mesoporous silica membrane (VMSM) as a molecular sieve and CRISPR trans-cleavage activity modulator, the system achieves precise regulation of $Ru(bpy)_3^{2+}$ adsorption *via* LPS-suppressed HCR assembly. This architecture enables physical confinement-mediated electrochemiluminescence (ECL) and fluorescence (FL) signal transduction, with dual-mode outputs providing mutual validation for enhanced reliability. The biosensor exhibits superior sensitivity with detection limits of 3.4 pg mL^{-1} for ECL and 1.4 pg mL^{-1} for FL, while also offering a broad dynamic range (0.005–100 ng mL^{-1}), significantly outperforming conventional LPS assays. The CRISPR-triggered HCR cascading G-wire dual amplification synergizes with nanoconfinement of VMSM to ensure robust anti-interference performance in complex matrices, validated by recovery rates of 97.8–102.5% in real samples. By integrating CRISPR programmability with nanoengineered signal amplification, this work establishes a transformative paradigm for portable, high-precision endotoxin detection in clinical diagnostics, industrial monitoring, and environmental safety applications.

Received 19th February 2025,
Accepted 13th March 2025

DOI: 10.1039/d5an00184f

rsc.li/analyst

1. Introduction

Lipopolysaccharides (LPS), as a critical structural component of the cell walls of Gram-negative bacteria, possess potent endotoxic activities.[1] Research has demonstrated that even at extremely low concentrations (*e.g.*, 1 ng kg^{-1} h^{-1}), LPS can trigger significant inflammatory responses in humans. Conversely, high-dose exposure may lead to life-threatening complications such as septic shock and multiple organ failure.[2,3] This strong pathogenic potential renders endotoxin detection a crucial quality control step in pharmaceutical production, medical device manufacturing, and food safety monitoring.[4] Currently, conventional detection methods for LPS mainly depend on the immunofluorescence assay and limulus amoebocyte lysate (LAL) test.[5,6] Despite their widespread adoption, these methods are constrained by labor-intensive workflows, prolonged analysis times, and vulnerability to matrix interference (*e.g.*, proteases, β-glucans), particularly in complex biological samples.[7,8] There is an urgent need for the development of an efficient, sensitive, and versatile method for detecting endotoxins in various sample types.

As biosensor technology continues to advance, the CRISPR (clustered regularly interspaced short palindromic repeats) system has established itself as a groundbreaking approach in molecular detection. CRISPR serves as a built-in defense mechanism found in bacteria that identifies and degrades foreign genetic material, such as viral DNA, through specific proteins like Cas12a.[9,10] Notably, the CRISPR/Cas12a system has garnered significant attention due to its programmable recognition capability based on trans-cleavage activity.[11] In this system, the Cas12a protein, directed by CRISPR RNA (crRNA), can specifically recognize and cleave non-specific

[a]*Key Laboratory of Interfacial Reaction & Sensing Analysis in Universities of Shandong, School of Chemistry and Chemical Engineering, University of Jinan, Jinan 250022, P. R. China. E-mail: chm_gaozf@ujn.edu.cn*
[b]*Department of Chemistry, Sungkyunkwan University, Suwon 16419, Republic of Korea*
[c]*State Key Laboratory of Analytical Chemistry for Life Science, Department of Chemistry, Nanjing University, Nanjing 210023, P. R. China*
† Electronic supplementary information (ESI) available. See DOI: https://doi.org/10.1039/d5an00184f

single-stranded DNA near target DNA sequences.[12,13] This unique functionality has opened possibilities for the development of biosensors based on CRISPR/Cas12a, which employ various detection methods, including fluorescence (FL),[14] electrochemiluminescence (ECL),[15] colorimetry,[16] and electrochemistry.[17,18] However, most existing biosensors rely on a single signal output mode, a design that is susceptible to interference from detection procedures and contaminating substances. This may lead to incorrect diagnoses, which include false positives or false negatives. Therefore, the design and development of a dual-modality sensing platform integrated with the CRISPR/Cas12a system are of great significance for enhancing the reliability of detection and broadening its application scope.

Although CRISPR-based systems are highly specific, single-mode detection remains vulnerable to environmental interference. To address this limitation, dual-mode systems provide self-validating signals, thereby enhancing detection reliability.[19] In recent years, researchers have developed various CRISPR/Cas12a-driven dual-modality detection systems, among which the integration of fluorescence (FL) with colorimetric analysis,[20–22] FL with electrochemical analysis,[23,24] and surface-enhanced Raman scattering (SERS) analysis serve as representative examples.[25,26] However, these systems typically require distinct molecular reporters for each detection mode, which can result in signal inconsistencies and complicate the workflow.[27] The FL-ECL approach, in contrast, offers several unique advantages.[28] This approach employs a single multifunctional indicator, such as luminol, iridium complexes, or quantum dots, to simultaneously output signals from the two detection modalities.[29] This design simplifies the experimental workflow and ensures consistency in the signal ratio between the two detection modes, effectively avoiding the common measurement inconsistencies associated with traditional dual-reporter systems.[30] Compared to conventional methods, the FL-ECL method offers distinct advantages. Traditional methods often rely on subjective visual interpretation for colorimetric readings or face challenges such as limited sensitivity and potential cross-interference between fluorescence and electrochemical signals. Additionally, fluorescence-SERS and electrochemical-SERS systems may encounter issues related to signal reproducibility and instrument complexity.[31–33] In contrast, the FL-ECL method enables quantitative measurements in complex matrices while maintaining stable performance. The fluorescence-ECL system achieves mutual validation through dual-signal output: fluorescence signals can monitor bioenzyme activity in real time, while ECL signals provide high sensitivity and specificity for target detection.[34] The integration of fluorescence measurements' established features with quantitative ECL data supports standardized practices across various laboratories. Additionally, the dual-signal fluorescence-ECL method employs cross-validation to ensure quality control, thereby significantly improving the accuracy and reliability of the detection results.

Herein, we develop a CRISPR/Cas12a-powered nanoconfined biosensing paradigm that hybrid chain reaction (HCR) cascading guanine nanowire (G-wire) dual amplification with mesoporous nanoengineering for ultrasensitive dual-mode LPS detection. By using vertically ordered mesoporous silica membrane (VMSM) as molecular sieves and CRISPR trans-cleavage activity modulators, the system achieves precise control over $Ru(bpy)_3^{2+}$ adsorption *via* LPS-suppressed HCR assembly, enabling physical confinement-mediated ECL-FL signal transduction. The inverse correlation between ECL attenuation (due to $Ru(bpy)_3^{2+}$ depletion from VMSM) and FL enhancement (from $Ru(bpy)_3^{2+}$-DNA complex formation) provides built-in self-validation, minimizing false signals. This nanoarchitecture attains low sensitivity across wide dynamic range, surpassing conventional LPS assays in both detection span and anti-interference capacity. The demonstrated integration of CRISPR programmability with ordered nanomaterial confinement effects establishes a transformative blueprint for portable endotoxin detection in clinical emergencies, industrial inspections, and environmental diagnostics.

2. Experimental section

2.1 Reagents and apparatus

Materials and instruments are listed in the ESI.†

2.2 Preparation of NH_2-VMSM/ITO

A precursor solution was prepared by mixing 20 mL of 0.1 M $NaNO_3$ with 20 mL ethanol, followed by sequential addition of 2.73 mL TEOS and 0.32 mL APTES under stirring. CTAB (68.17 mg, 4.35 mM final concentration) was then incorporated, with pH adjusted to 3 using 6 M HCl. After 2.5 h hydrolysis at room temperature, the film was electrodeposited using a three-electrode system (−0.70 mA cm^{-2}, 5 s). The resulting electrode was rinsed with ultrapure water, N_2-dried at 120 °C, and aged overnight. Template removal was achieved by 5 min immersion in 0.1 M HCl/ethanol solution.

2.3 Preparation of Ru-VMSM/ITO

A 1 mg mL^{-1} $Ru(bpy)_3^{2+}$ solution was prepared by dissolving 40 mg tris(2,2′-bipyridyl) ruthenium(II) chloride hexahydrate in 40 mL pH 8.0 PBS. Electrophoretic deposition was performed under cathodic polarization (−1.0 V *vs.* Ag/AgCl, 40 s) using the same three-electrode configuration, with 10 μM $Ru(bpy)_3^{2+}$ in 10 mM PBS (pH 8.0). Post-deposition rinsing with ultrapure water yielded the final Ru-VMSM/ITO platform.

2.4 Process of HCR cascading G-wire amplification

The experimental buffer consists of 10 mM Tris-HCl, with 100 mM NaCl and 150 mM KCl. The procedure involves mixing 6 μL of LPS aptamer AP (0.6 μM) with 10 μL of LPS at varying concentrations in a centrifuge tube using a microliter pipette. The mixture is then diluted to a final volume of 100 μL using the buffer and labeled from A to G. These mixtures are incubated at 37.0 °C for 1.5 h. Subsequently, 50 μL of each

solution is transferred to a new centrifuge tube, where 0.25 μL of Cas12a (200 nM), 20.0 μL of RNAse inhibitor (80 U), 2.0 μL of crRNA (200 nM), and 25.0 μL of the oligomer synthesized from H1, H2, T, and c-myc are added. The mixture is made up to a total volume of 100 μL using buffer, and then maintained at 37.0 °C for 30.0 min. Following this, 50 μL of the incubated solution is transferred to another centrifuge tube, and 50.0 μL of $MgCl_2$ solution is added. The resulting mixture is incubated at 37.0 °C for an additional 30.0 min to facilitate the formation of hyperbranched nucleic acid topological structures. Finally, the mixture is heated at 65.0 °C for 10.0 min to inactivate Cas12a.

2.5 ECL measurements

After constructing hyperbranched nucleic acid topological structures, they were added to an electrochemical cell containing 10 mL of PBS buffer solution (10 mM, pH = 8.0) and subjected to ECL measurements using a three-electrode system. ECL signals were obtained using cyclic voltammetry (0 to 1.2 V, 0.15 V s^{-1}), with the photomultiplier tube voltage set to 800 V. Subsequently, the solution from the electrolytic cell was used to detect the absorption of Ru by the hyperbranched nucleic acid topological structures, thereby achieving the precise detection of LPS.

3. Results and discussion

3.1 Principle of the FL-ECL dual-mode biosensor for LPS detection

As illustrated in Scheme 1, the mechanism of the VMSM-based FL-ECL dual-mode biosensor, integrated with the CRISPR/Cas12a system, for LPS detection is presented. Initially, negatively charged VMSM is prepared to attract the positively charged luminescent agent $Ru(bpy)_3^{2+}$ through electrostatic interactions, enabling it to be confined within the pores. After the addition of co-reactant tripropylamin (TPrA), significant ECL was observed due to the oxidation–reduction reaction between TPrA and $Ru(bpy)_3^{2+}$. The aptamer (APT) probe was designed with dual functions that enhance the recognition of CRISPR/Cas12a and to specifically combine with LPS with high affinity. The crRNA was designed to hybridize with an LPS-binding aptamer-DNA conjugate, enabling Cas12a activation only in the absence of LPS. In the presence of LPS, the APT preferentially and specifically binds to LPS, resulting in the inactivation of CRISPR/Cas12a and preventing it from cleaving the substrate nucleic acid probes. Thus, the HP1 probe that has the complementary region with T probe could hybridize with HP2 probe, which in turn open up HP1 probe again and initiate the HCR reaction. Notably, free parts of HP1 and HP2 enable the formation of G-quadruplex in the presence of K^+, which could be extended to generate the G-wire complex structure with the assistance of Mg^{2+}. Thus, highly negatively charged hyperbranched DNA structure was formed, which facilitates the competitive adsorption of the positively charged $Ru(bpy)_3^{2+}$ into it, thereby reducing the ECL intensity of VMSM and enhancing the FL intensity of the solution. Conversely, the APT probe could effectively bind with Cas12a/crRNA to active the trans-cleaving activity of CRISPR/Cas12a system, digesting all the probe substrates into fragments. Thus, the luminescent agents remain restrained inside the VMSM, producing high ECL intensity in the biosensing interface and low FL in the solution. By observing the opposite changes in fluorescence and electrochemiluminescence signals, the exact level of LPS can be measured. This biosensor integrates the precise targeting ability of CRISPR/Cas12a along with enhanced signal amplification through HCR and G-wire mechanisms, offering a robust system for accurately detecting LPS.

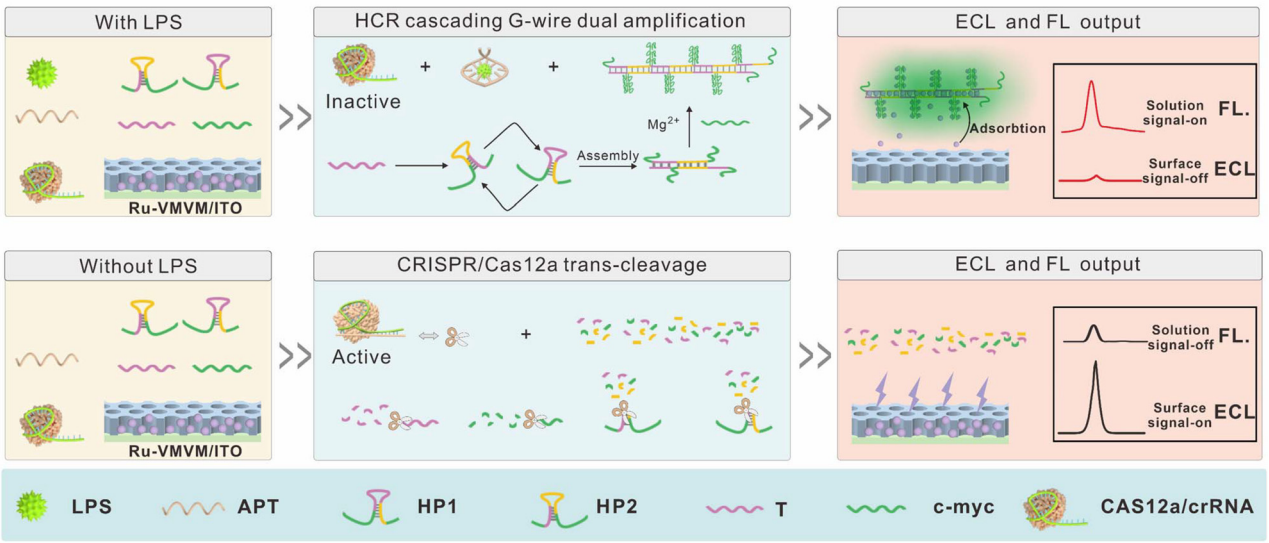

Scheme 1 The conceptual framework for a dual-signal optical biosensor that employs fluorescence and electrochemiluminescence.

3.2 Feasibility analysis of the proposed method

To assess the HCR cascading G-wire dual amplification strategy, a gel electrophoresis experiment was conducted (Fig. 1A). Substrates, including HP1, HP2, T, and c-myc, exhibited rapid migration in lanes 1, 2, 3, and 5, respectively, due to their low molecular weights. In contrast, the HCR products displayed a higher molecular weight, resulting in significantly slower migration in lane 4. In lane 6, the DNA architecture constructed *via* sequential HCR and G-wire assembly demonstrated the lowest electrophoretic mobility, consistent with the formation of high-molecular-weight nanostructures. This observation confirmed that the HCR cascading G-wire dual amplification strategy successfully initiated and generated a high dimensional structure with high molecular weight.

Next, we aimed to evaluate the feasibility of the proposed method for LPS detection by FL and ECL signals. In the absence of LPS, the ECL intensity was primarily associated with the electrophoretic deposition of Ru alone, yielding a strong ECL signal alongside a weak FL signal. However, upon the addition of LPS, we observed a similar pattern of weak ECL intensity and strong FL signal, which is critical for sensor detection (Fig. 1B and C). To evaluate the ability of signal amplification, the HCR single amplification was conducted as a control. As shown in Fig. 1D and E, the FL only increased 196.55%, which is much lower than that HCR cascading G-wire dual amplification (567.24%). Moreover, the ECL signal decreased from 1.61k to 0.98k, with 39.13% reduction by the HCR single amplification. Impressively, the ECL alteration increased to 71.09% when we employ the HCR cascading G-wire dual amplification. Therefore, our findings show that the developed approach can successfully enhance both FL and ECL signals, making it suitable for detecting low concentrations of LPS.

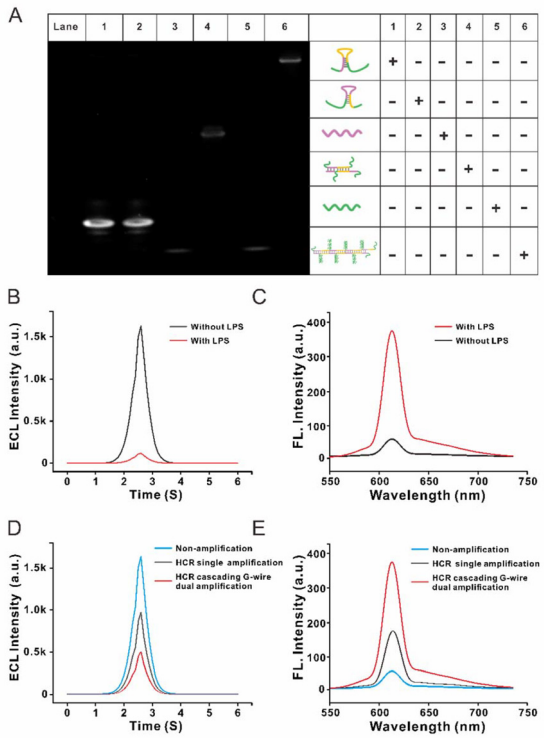

Fig. 1 (A) Gel electrophoresis analysis of HCR cascading G-wire amplification products. Lane 1: HP1; lane 2: HP2; lane 3: T; lane 4: HCR product; lane 5: c-myc; lane 6: G-wire assembly. (B) ECL and (C) FL signal responses to LPS (0 *vs.* 100 ng mL^{-1}). (D) ECL and (E) FL signal amplification efficiency comparison between HCR-only and HCR cascading G-wire strategies.

3.3 Characterization of VMSM

To verify the nanostructure of VMSM, a series of characterizations were conducted. First, transmission electron microscopy (TEM) image was employed to obtain the morphological information of VMSM. In Fig. 2A and S1,† VMSM showed a regular SiO_2 nanopore array structure, indicated the porous dispersion and uniformity of SiO_2. The scanning electron microscope (SEM) cross-sectional image in Fig. 2B confirmed the successful deposition of the SiO_2 layer approximately 50 nm thick on the ITO electrode. The presence of nanopores in the structure provided a potential site for the adsorption of ruthenium ions within the pores. Furthermore, the crystal structure of SiO_2 was analyzed using X-ray diffraction (XRD). As shown in Fig. 2C, diffraction peaks at 2θ values of 21.0°, 26.4°, and 42.1° corresponded to the (100), (101), and (200) crystal planes of SiO_2 (PDF#64-7406), respectively. Finally, the surface chemistry of SiO_2 was investigated by X-ray photoelectron spectroscopy (XPS). The XPS spectra (Fig. 2D) revealed prominent peaks for Si and O, confirmed the presence of these elements in the material. In the Si 2p spectrum (Fig. 2E), the characteristic peak at 103.4 eV was assigned to the Si 2p orbital. As shown in Fig. 2F, the peak at 532.3 eV in the O 1s spectrum was attributed to the lattice oxygen in SiO_2, and the characteristic peak of binding energy of 533 eV came from the adsorbed oxygen on the surface. All of the above results demonstrated that the preparation of the VMSM was successful.

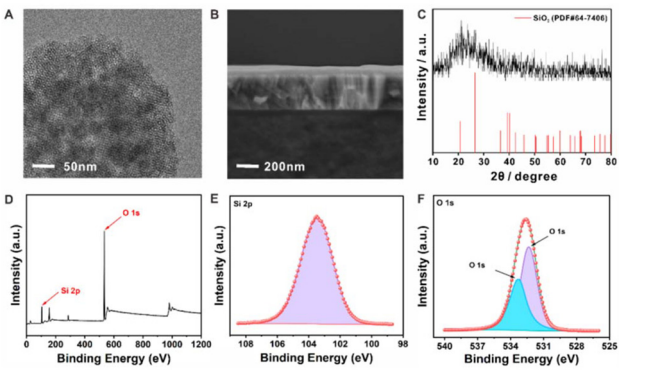

Fig. 2 Characterization of VMSM. (A) TEM analysis of VMSM. (B) Cross-sectional SEM analysis of VMSM. (C) XRD analysis of VMSM. XPS analysis of (D) VMSM, (E) Si 2p, and (F) O 1s.

3.4 Investigation of the luminescence mechanism

To investigate the luminescence mechanism of the sensor, cyclic voltammetry (CV) curves and ECL responses were plotted. As illustrated in Fig. 3A, compared to VMSM, further modification with $Ru(bpy)_3^{2+}$ leads to an increase in the peak current density. However, when LPS is present in the solution, the DNA scaffold undergoes a conformational change that promotes the adsorption of $Ru(bpy)_3^{2+}$ complexes and their spatial sequestration within the HCR cascading G-wire products. This process restricts the accessibility of $Ru(bpy)_3^{2+}$ to the electrode surface, thereby reducing the current density. Additionally, a similar trend observed in the CV curves (Fig. 3B), indicating that the hyperbranched DNA products generated with the addition of LPS effectively adsorbs $Ru(bpy)_3^{2+}$ into the solution, resulting in significant signal changes. CV and EIS experiments were conducted to verify the sensor construction process. As illustrated in Fig. 3C and D, it was observed that the current density increases and the resistance (R_{et}) decreases when Ru is electrodeposited onto the VMSM/ITO surface. However, when the solution contains LPS, $Ru(bpy)_3^{2+}$ transfers from the VMSM to the HCR cascading G-wire products, leading to a further decrease in current density and a gradual increase in resistance. The CV and EIS measurements confirmed the successful construction of the sensor.

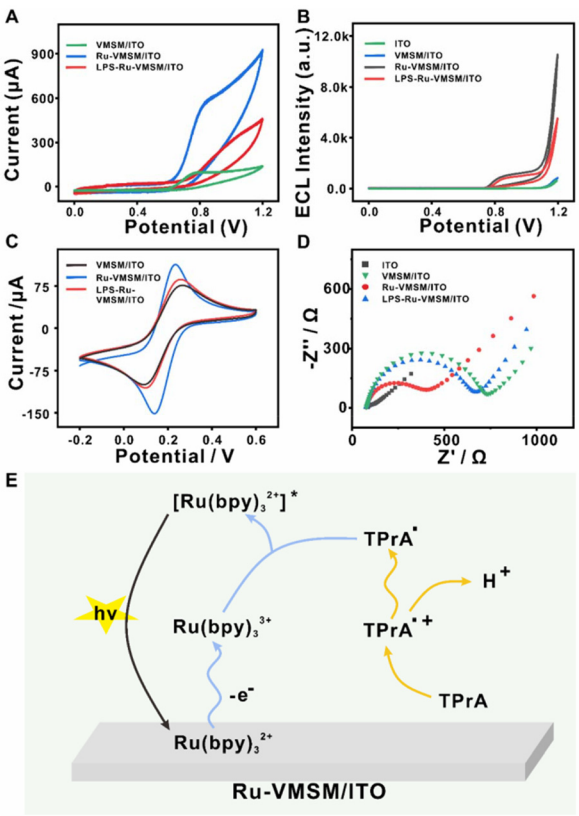

Fig. 3 (A) CV curves of VMSM/ITO, Ru-VMSM/ITO, and LPS-Ru-VMSM/ITO. (B) ECL responses of ITO, VMSM/ITO, Ru-VMSM/ITO, and LPS-Ru-VMSM/ITO. (C) CV curves of VMSM/ITO, Ru-VMSM/ITO, and LPS-Ru-VMSM/ITO. (D) EIS responses of ITO, VMSM/ITO, Ru-VMSM/ITO, and Ru-VMSM/ITO. (E) Possible ECL mechanism Ru-VMSM/ITO.

Based on the aforementioned research, the reaction mechanism of the sensor is illustrated in Fig. 3E. The ECL mechanism involves synergistic interactions between TPrA (co-reactant) and $Ru(bpy)_3^{2+}$ (lumophore): TPrA undergoes initial electrochemical oxidation to form $TPrA^{\bullet+}$ which subsequently deprotonates to produce strongly reducing $TPrA^{\bullet}$ radicals (eqn (1) and (2)). Simultaneously, $Ru(bpy)_3^{2+}$ is electrochemically oxidized to $Ru(bpy)_3^{3+}$ (eqn (3)). These oxidized $Ru(bpy)_3^{3+}$ species then accept electrons from $TPrA^{\bullet}$ radicals through a redox annihilation process, promoting the luminophore to its excited state $[Ru(bpy)_3^{2+}]^*$ (eqn (4)). The system finally achieves ECL emission *via* radiative relaxation of the excited state, with TPrA acting as the radical precursor and $Ru(bpy)_3^{2+}$ serving as both electron acceptor and light emitter (eqn (5)).

$$TPrA\text{-}e^- \rightarrow TPrA^{\bullet+} \quad (1)$$

$$TPrA^{\bullet+}\text{-}e^- \rightarrow TPrA^{\bullet} + H^+ \quad (2)$$

$$Ru(bpy)_3^{2+}\text{-}e^- \rightarrow Ru(bpy)_3^{3+} \quad (3)$$

$$Ru(bpy)_3^{3+} + TPrA^{\bullet} \rightarrow [Ru(bpy)_3^{2+}]^* \quad (4)$$

ECL emission:

$$[Ru(bpy)_3^{2+}]^* \rightarrow Ru(bpy)_3^{2+} + h\nu \quad (5)$$

3.5 Optimization of experimental conditions

To optimize the sensing capabilities of the system, a range of operating parameters were systematically fine-tuned. The assembly time of the amplification process, which in turn influences the absorption efficiency of $Ru(bpy)_3^{2+}$ and ultimately impacts the ECL intensity. Therefore, we conducted a condition selection experiment for this factor, with results shown in Fig. S2 and S3.† The results indicate that before 50 min, the ECL signal intensity decreases as the assembly time of the HCR cascading G-wire dual amplification increases, while the FL signal intensity increases, reaching a plateau after 50 min. Consequently, we conclude that the optimal assembly time for the hyperbranched structure is 50 min. The pH value of the Tris-HCl buffer affects the construction of the hyperbranched nucleic acid topology, thereby influencing its absorption efficiency of $Ru(bpy)_3^{2+}$ and ultimately impacting the ECL intensity. Therefore, we performed a selective experiment on the pH value of the Tris-HCl buffer. Under the same LPS concentration, hyperbranched nucleic acid topologies were constructed using Tris-HCl buffers with pH values of 7.4, 7.6, 7.8, 8.0, 8.2 and 8.4, followed by ECL and FL detection. The results shown in Fig. S4 and S5† indicate that the ECL and FL signal responses are strongest when the pH value of the Tris-HCl buffer is 8.0. Thus, the optimal pH value for the Tris-HCl buffer is 8.0.

3.6 Detection of LPS using the proposed platform

Under the optimized experimental conditions, we assessed the functionality of the FL-ECL dual-mode biosensor we designed for detecting LPS. Fig. 4A and D indicate that the ECL signal intensity gradually decreases while the FL signal intensity gradually increases with the increase in LPS concentration from 0.0005 to 100 ng mL^{-1}. The quantitative relationships can be read from Fig. 4B, C, E and F. We observed that both ECL and FL signal intensities exhibit a linear relationship with the logarithm of LPS concentration. The ECL signal exhibited a linear correlation with the logarithm of LPS concentration (0.005–100 ng mL^{-1}) following the equation: $I = -2373.29 \lg c_{LPS} + 11\,040.06$ ($R^2 = 0.9961$), achieving a detection limit (LOD) of 3.4 pg mL^{-1} (S/N = 3). Similarly, the FL response adhered to $I = 40.1017 \lg c_{LPS} + 291.9192$ ($R^2 = 0.9862$), with an LOD of 1.4 pg mL^{-1}. These results confirm the superiority of the proposed dual-mode sensor in LPS detection.

The dual-mode biosensor proposed in this study, as detailed in Table S2,† exhibits superior analytical performance compared to earlier detection methods. This enhancement stems from multiple factors. The HCR-mediated G-wire dual amplification strategy effectively boosts both FL and ECL signals, thereby enhancing sensitivity. Furthermore, the CRISPR mechanism facilitates enhanced signal amplification *via* its indiscriminate trans-cleavage function, enabling sustained ssDNA substrate degradation triggered by a singular recognition event.

3.7 Investigation of selectivity and practicability

Various performances, including stability, selectivity, and practicability, were comprehensively investigated. First, the test stability of the constructed biosensor was quite excellent in the presence of different concentrations of LPS (Fig. S6†). After detection for 7 days consecutively on several electrodes with the same modification conditions, the results of ECL response showed that the storage stability was also outstanding (Fig. S7†). The specificity of the dual-mode biosensor was assessed by introducing various interfering substances into the analytical system, including glucose (Glu), lactose (Lac), L-leucine (Leu), L-alanine (Ala), and a blank control. After the reaction was completed, we detected the ECL and FL signals of the products. The results, shown in Fig. S7 and S8,† indicate that only the ECL and FL signal intensities of the LPS group exhibited significant differences, while the signal intensities of the other additive groups were not significantly different from the control group. Throughout the detection period, the ECL signal intensity changes across different concentrations were not significant, indicating that the sensor prepared in this experiment has good reproducibility. Five measurements were performed on the same ECL sensor, as shown in Fig. S9 and S10.† There were no significant differences among the five ECL signals, indicating that the sensor has good reproducibility. This result suggests that the sensor is minimally affected by other potential interfering substances during detection, allowing us to confirm its excellent performance.

To evaluate the feasibility of the developed sensing approach in real-world biological samples, we introduced different concentrations of LPS into real samples for recovery experiments. Human serum samples were pre-filtered (0.22 μm) and diluted 10-fold in PBS (pH 8.0) to mitigate matrix interference prior to spiking with LPS. As shown in Table 1, the recovery rates ranged from 97.8% to 102.5%, with all experiments having a relative standard deviation (RSD) of less than 5%. The findings in Table S2† reveal notable improvements in sensitivity and an extensive linear range, suggesting that the method holds promising potential for the highly sensitive detection of LPS. Additionally, the developed biosensor's ability to detect LPS in real-world samples further confirms the accuracy and reliability of the proposed biosensing system.

Table 1 The results of the LPS determination in diluted human serum (10-fold) samples

Samples	Added (ng mL^{-1})	Detected (ng mL^{-1}, n = 5)	RSD (%)	Recovery (%)
0.6	0.40	1.01	4.7	102.5
	0.90	1.51	1.4	101.1
	1.40	1.98	4.9	98.6
10.0	5.00	14.89	1.8	97.8
	10.00	20.06	2.6	100.3
	15.00	24.97	4.3	99.9

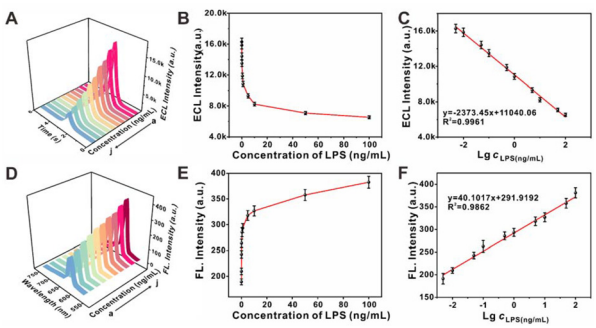

Fig. 4 (A) Plot showing ECL responses to varying LPS concentrations, ranging from 0.005 to 100 ng mL^{-1}. (B) Graph illustrating the direct relationship between ECL intensity and LPS concentration. (C) Calibration plot demonstrating the linear relationship between ECL intensity and LPS concentration. (D) Plot displaying fluorescence responses to varying LPS concentrations, from 0.005 to 100 ng mL^{-1}. (E) Graph showing the direct relationship between fluorescence intensity and LPS concentration. (F) Calibration plot illustrating the linear relationship between fluorescence intensity and LPS concentration. Error bars: SD (n = 5).

4. Conclusions

In summary, we present a novel nanoconfined dual-mode biosensing strategy based on the CRISPR/Cas12a system. Leveraging the molecular store effect of VMSM coupled with HCR cascading G-wire dual amplification, the platform

enables precise regulation of CRISPR trans-cleavage activity triggered by LPS. Innovatively, the adsorption–desorption behavior of $Ru(bpy)_3^{2+}$ synchronously drives dual-channel signal outputs in FL and ECL, overcoming the bottleneck of signal mismatch caused by multiple molecular probes in conventional dual-mode detection. Experimental results demonstrate pg mL^{-1}-level sensitivity and a wide dynamic range for LPS detection, along with exceptional anti-interference capability in complex matrices. The FL-ECL dual-modal signals achieve mutual validation through real-time enzymatic activity monitoring and high-sensitivity quantitative detection, significantly enhancing result reliability. This work establishes a paradigm for synergistic innovation between CRISPR-based biosensing and nanoconfined engineering, potentially advancing portable endotoxin detection technologies in clinical emergency settings, industrial monitoring, and environmental diagnostics.

Data availability

The data underlying this article are available in the article and in its ESI.†

Conflicts of interest

There are no conflicts to declare.

Acknowledgements

This work was supported by the National Natural Science Foundation of China (22176080), Natural Science Foundation of Shandong Province (ZR2023YQ015), and the Taishan Scholar Project of Shandong Province (tsqn202312216).

References

1 F. Di Lorenzo, K. A. Duda, R. Lanzetta, A. Silipo, C. De Castro and A. Molinaro, *Chem. Rev.*, 2022, **122**, 15767–15821.
2 L. Perea, M. Coll, L. Sanjurjo, D. Blaya, A. E. Taghdouini, D. Rodrigo-Torres, J. Altamirano, I. Graupera, B. Aguilar-Bravo, M. Llopis, J. Vallverdú, J. Caballeria, L. A. van Grunsven, M.-R. Sarrias, P. Ginès and P. Sancho-Bru, *Hepatology*, 2017, **66**, 953–968.
3 W.-C. Geng, Z. Zheng and D.-S. Guo, *VIEW*, 2021, **2**, 20200059.
4 S. Shen, F. Han, A. Yuan, L. Wu, J. Cao, J. Qian, X. Qi, Y. Yan and Y. Ge, *Biomaterials*, 2019, **189**, 60–68.
5 C. Zhang, F. Tian, M. Zhang, Z. Zhang, M. Bai, G. Guo, W. Zheng, Q. Wang, Y. Shi and L. Wang, *Sci. Total Environ.*, 2019, **681**, 365–378.
6 P. Zhu, V. A. Papadimitriou, J. E. van Dongen, J. Cordeiro, Y. Neeleman, A. Santoso, S. Chen, J. C. T. Eijkel, H. Peng, L. I. Segerink and A. Y. Rwei, *Sci. Adv.*, 2023, **9**, eadf5509.
7 H. Grallert, S. Leopoldseder, M. Schuett, P. Kurze and B. Buchberger, *Nat. Methods*, 2011, **8**, iii–v.
8 W. Su and X. Ding, *SLAS Technol.*, 2015, **20**, 354–364.
9 N. Akimov, J. Scudder and J. Y. Ye, *Biosens. Bioelectron.*, 2021, **191**, 113436.
10 B. F. Far, M. R. Naimi-Jamal, S. Ahmadi and N. Rabiee, *Nano Mater. Sci.*, 2024, DOI: 10.1016/j.nanoms.2024.06.004.
11 L. Xu, S. Liu, Z. Huang, X. Pei, S. Li, Y. He, Y. Tong and G. Liu, *J. Anal. Test.*, 2024, **9**, 153–159.
12 R. Fu and Y. Xianyu, *Small*, 2023, **19**, 2300057.
13 Y. Xie, H. Li, F. Chen, S. Udayakumar, K. Arora, H. Chen, Y. Lan, Q. Hu, X. Zhou, X. Guo, L. Xiu and K. Yin, *Adv. Sci.*, 2022, **9**, 2204172.
14 J.-H. Choi, J. Lim, M. Shin, S.-H. Paek and J.-W. Choi, *Nano Lett.*, 2021, **21**, 693–699.
15 M.-L. Liu, Y. Li, M.-L. Zhao, Y. Zhuo and X.-J. He, *Biosens. Bioelectron.*, 2022, **214**, 114512.
16 H. Jiang, S. Qi, I. M. Khan, X. Dong, Z. Wang and J. Yang, *Sens. Actuators, B*, 2024, **414**, 135969.
17 H. Duan, Y. Wang, S.-Y. Tang, T.-H. Xiao, K. Goda and M. Li, *Sens. Actuators, B*, 2023, **380**, 133342.
18 Y. Du, S. Ji, Q. Dong, J. Wang, D. Han and Z. Gao, *Anal. Chim. Acta*, 2023, **1245**, 340864.
19 F. Liu, J. Zhao, X. Liu, X. Zhen, Q. Feng, Y. Gu, G. Yang, L. Qu and J.-J. Zhu, *Anal. Chem.*, 2023, **95**, 14297–14307.
20 Q. Wei, X. Zhu, D. Zhang, H. Liu and B. Sun, *Trends Food Sci. Technol.*, 2024, **151**, 104636.
21 G. Mao, X. Luo, S. Ye, X. Wang, J. He, J. Kong, J. Dai, W. Yin and Y. Ma, *Anal. Chem.*, 2023, **95**, 8063–8069.
22 S. Zhou, J. Dong, L. Deng, Z. Huang, P. Lu, G. Wang, M. Yang, D. Huo and C. Hou, *Sens. Actuators, B*, 2023, **392**, 134034.
23 Q. Pu, Y. Ye, J. Hu, C. Xie, X. Zhou, H. Yu, F. Liao, S. Jiang, L. Jiang, G. Xie and W. Chen, *Talanta*, 2023, **252**, 123754.
24 C. Wang, W. Ma, T. Jia, X. Zhang and X. Fan, *Sens. Actuators, B*, 2025, **422**, 136452.
25 J. Liu, J. Chen, D. Wu, M. Huang, J. Chen, R. Pan, Y. Wu and G. Li, *Anal. Chem.*, 2021, **93**, 10167–10174.
26 F. Arshad, A. N. Abdillah, P. Shivanand and M. U. Ahmed, *Biosens. Bioelectron.*, 2024, **247**, 115940.
27 Y. Xu, J. Ma, C. Dai, Z. Mao and Y. Zhou, *Biosens. Bioelectron.*, 2024, **264**, 116678.
28 H. Sun, J. Guan, H. Chai, K. Yu, L. Qu, X. Zhang and G. Zhang, *Biosens. Bioelectron.*, 2024, **251**, 116080.
29 X. Wang, H. Chen, M. Sun, B. Chen, H. Xu, Y. Fan, H. Zhou and J. Liu, *Sens. Actuators, B*, 2025, **425**, 137016.
30 H. Gao, H. Zhang, X. Qi, M. Miao, L. Que, X. Gu, D. Chang and H. Pan, *Talanta*, 2025, **282**, 127013.
31 L. Huang, H. Huang, Z. Zhang and G. Li, *Anal. Chem.*, 2023, **95**, 5946–5954.
32 L. Qin, T. Huang, H. Cui, M. Cheng, G. Wei, F. Liao, W. Xiong, H. Jiang, J. Zhang and H. Fan, *Biosens. Bioelectron.*, 2023, **235**, 115385.
33 Z. Lu, W. Ni, N. Liu, D. Jin, T. Li, K. Li, Y. Zhang, Q. Yao and G.-J. Zhang, *Microchem. J.*, 2023, **187**, 108370.
34 K. Zhang, Z. Fan, B. Yao, Y. Ding, J. Zhao, M. Xie and J. Pan, *Biosens. Bioelectron.*, 2021, **178**, 113019.